Differential cross sections for the multiple ionization of Ne and Ar by protons

Alejandro D. González and Erik Horsdal Pedersen
Institute of Physics and Astronomy, Aarhus University, DK-8000 Aarhus C, Denmark
(Received 7 July 1993)

Differential cross sections $d\sigma^{q+}(E,\varphi)/d\Omega$ for multiple ionization of Ne and Ar by protons have been measured for final charge states $q=1-6$, impact energies $E=0.4-3$ MeV, and scattering angles $\varphi=0.28-6.5$ mrad. Within these ranges of energies and scattering angles, the angular dependence of the differential cross section for single ionization at constant energy follows a power law, $d\sigma^{+}/d\Omega \propto \varphi^{-k}$. The power k is found to be near 3.8 for Ne and 3.65 for Ar. A monotonic increase of all the *multiple-ionization* cross sections $d\sigma^{q+}/d\Omega$, $q \geq 2$ relative to the *single-ionization* cross section $d\sigma^{+}/d\Omega$, is observed for increasing scattering angle. This behavior is most likely due to the combined effect of two multiple-ionization mechanisms. At the most distant collisions, the multiple ionization is dominated by the direct removal of valence electrons by the projectile. At the closest collisions, inner-shell ionization, followed by vacancy cascades, adds to the production of high-charge states. For Ne, this interpretation is supported by qualitative agreement with a model calculation based on the assumption that the multiple ionization of each shell follows binomial statistics. Quantitative agreement between experiment and theory requires a more thorough analysis of the many-body problem.

PACS number(s): 34.50.Fa

INTRODUCTION

The ultimate state of ionization of a target atom after a fast collision with an ion is determined by the combined effect of prompt and delayed ionization. The prompt ionization results not only from the (multiple) interaction between the projectile and the target electrons but also from the interaction among the target electrons themselves during the collision. Prompt multiple ionization of outer shells by heavy ions at small impact parameters has been studied by high-resolution x-ray or Auger-electron spectroscopy of inner-shell satellite lines [1,2], and the interaction between the valence-shell electrons is most likely essential for double ionization of the noble gases, in particular He, by fast, light ions (protons, antiprotons, or α particles [3]), or by high-energy photons [4]. The delayed ionization is a result of the rearrangement of the excited-target-electron cloud after the collision. It is particularly effective in producing high-charge states when a hole is formed in an inner shell. The hole often decays through a series of radiationless transitions by which several electrons are ejected into continuum states. The delayed ionization is seen most clearly in studies of multiple ionization following photoionization of inner shells [5].

In the general case, where different multiple-ionization mechanisms compete, total cross-section studies alone are not sufficient for a detailed, quantitative understanding of the multiple ionization. Experimental cross sections that are differential in the projectile scattering angle, $d\sigma^{q+}(E,\varphi)/d\Omega$, may help in the interpretation by separating close and distant collisions with respect to the various shells of the target atom.

In this publication, we present experimental data on the multiple ionization of Ne and Ar by protons in the velocity range 4–11 a.u. and for scattering angles in the range 0.28–6.5 mrad. The data show angularly dependent variations which are believed to reveal the transition from very distant collisions, where the ionization is dominated by direct ionization of electrons from the outermost shell, to closer collisions, for which the decay of inner-shell vacancies contributes significantly to the multiple ionization.

Kamber *et al.* [6] previously measured $d\sigma^{q+}(E,\varphi)/d\varphi = 2\pi\varphi d\sigma^{q+}(E,\varphi)/d\Omega$ for protons on Ne and Ar for charge states $q=1-3$, impact energies $E=3$ and 6 MeV, and deflection angles $\varphi=0.2-0.9$ mrad, and Sharabati *et al.* [7] measured angularly dependent multiple-ionization probabilities $P^{q+}(E,\varphi)$ for protons on Ne for $q=1-4$, $E=300-500$ keV, and $\varphi=3-10$ mrad. The present data are compared with these measurements where possible. Cross sections that are different in projectile scattering angle for single and double ionization of He by fast proton impact have been reported by Schiwietz [8], Kamber *et al.* [9], and Kristensen and Horsdal-Pedersen [10].

EXPERIMENTAL ARRANGEMENT AND PROCEDURES

The experimental arrangement used for the preset measurements is shown schematically in Fig. 1. The proton beam from a 5-MV single-stage Van de Graaff accelerator was collimated by two sets of adjustable apertures (typically 0.01×0.02 mm^2) separated by 2000 mm. After collimation, the protons were deflected by a magnetic field and directed through a gas cell with a 1-mm entrance and a 2-mm exit aperture. Ions formed in the gas cell were extracted electrostatically (40 V/cm in the cell) and, after further acceleration through a potential difference of 4.2 kV, counted by a secondary-electron multiplier at an energy of $4.2q$ keV, where $q=1-6$ is the charge state of the extracted ion. Scattered protons were detected 1893 mm downstream from the gas cell by a Si surface-barrier (SB) detector masked by a thin metal foil with a set of apertures (AP). The apertures are shown in the inset of Fig.

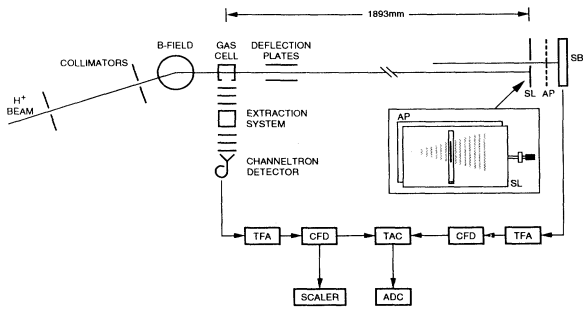

FIG. 1. Experimental arrangement consisting of collimating apertures for the proton beam, deflection magnet, gas cell, electrostatic target-ion extraction system, electrostatic deflectors, (SB) surface barrier detector for fast, scattered protons, secondary-electron multiplier for extracted recoil ions, (AP) apertures in front of SB defining a series of deflection angles, (SL) slit in front of AP used to select one particular deflection angle. The electronics consists of fast amplifiers (TFA), constant fraction discriminators (CFD), a time-to-pulse height converter (TAC), an analog-to-digital converter (ADC), and a scaler.

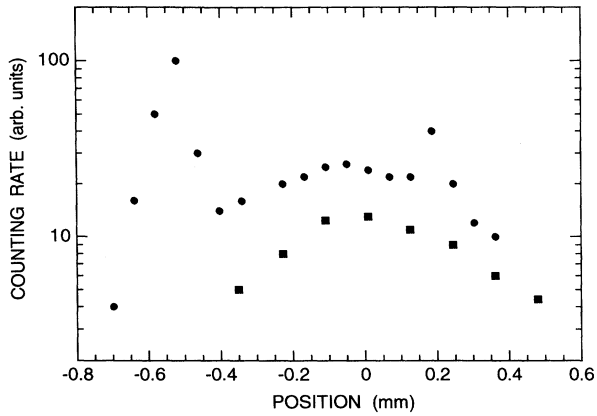

FIG. 2. Counting rate of detector SB as a function of horizontal position of the detector relative to a 1-MeV proton beam. The small circular hole was selected (see inset in Fig. 1). ●, discriminator (CFD in Fig. 1) set at 0.5 MeV; ■, discriminator set just below 1 MeV. The broad maximum of the two distributions at zero marks the horizontal position of the beam. The two narrow peaks on each side of the broad maximum seen in the upper curve are due to slit scattering from SL (see inset of Fig. 1).

1. There is one small circular aperture with a diameter of 0.37 mm and a series of rectangular apertures of width 0.37 mm and covering an angular region of 30°, as seen from the small circular hole. The apertures allowed selection of a number of discrete deflection angles $[(1.004+n\times0.475)$ mrad, $n=0,1,2,3,\ldots]$. The azimuthal angle was chosen such that the transverse momentum transfer from the projectile to the target atom was in the direction of the extraction. The aperture of interest was selected by a movable slit (SL) in front of the detector arrangement (see inset in Fig. 1). The detector was centered such that the direction of the main beam was towards the small circular hole. This was done by recording the counting rate of the detector while scanning the beam above or below the hole by means of electrostatic deflectors situated just behind the gas cell. The position of the maximum counting rate gives the center position in the horizontal direction. A similar procedure was used to find the vertical center position. Examples of horizontal scans are shown in Fig. 2. One scan is taken with the discriminator on the SB detector set just below the full-energy signal, while the other is taken with the discriminator set somewhat above the noise. Apart from the maximum seen in both curves, which gives the horizontal center position, the upper spectrum shows two peaks, one on each side of the maximum. These peaks are due to low-energy protons which were scattered off the edges of the movable SL (0.7 mm wide) in front of the detector. The sharpness of the edge of this slit varies along the slit and from one side to the other. This explains the difference in height of the two narrow peaks. There is also a slight misalignment of SL relative to the small circular hole, as seen from the asymmetric positions of the narrow peaks. This asymmetry was subsequently corrected. The widths of the two peaks give a measure of the width of the beam. The peaks are present only at high energies ($E\geq1$ MeV). At lower energies, the width of the beam was found by observing the current on a 0.1-mm-thick wire that could be scanned through the beam. The full width at half maximum (FWHM) of the beam at the detector was always found to be within the range 0.15–0.20 mm. Measurements at scattering angles in the range 0.3–1.0 mrad were done by selecting the small circular hole centered on the main, undeflected beam and deflecting the beam electrostatically through a carefully controlled angle by means of the deflection plates (see Fig. 1) situated close to the exit of the gas cell.

The scattering angle φ was found by averaging over the selected aperture and the beam profile using (in an iterative way) the measured differential cross section for single ionization $d\sigma^+(\varphi)/d\Omega$

$$\varphi=\frac{\int d^2A_a\int d^2A_b\varphi'\dfrac{d\sigma^+}{d\Omega}(\varphi')}{\int d^2A_a\int d^2A_b\dfrac{d\sigma^+}{d\Omega}(\varphi')}, \tag{1}$$

where $\int dA_a^2$ and $\int d^2A_b$ symbolize integration over aperture and beam, respectively. The beam profile was assumed to be Gaussian with a width $\sigma=0.42\times$FWHM and it was integrated to 3σ. The cross sections were assumed to follow a power law.

The averaged angle φ deviates from the geometrical angle φ_g (measured from the center of the beam to the center of the aperture) by about 1% or less for the rectangular apertures (angles larger than 1 mrad), but the deviation may be as high as about 15% for the smallest angles measured with the circular hole, as seen from the examples shown in Table I.

A coincidence technique employing a time-to-amplitude-converter (TAC) was used to identify extracted ions with the ionizing proton (see Fig. 1). The TAC was started by the detection of a scattered proton and stopped by the detection of the first subsequently extracted ion.

TABLE I. Averaged deflection angles.

Aperture (mm)	Width σ_B (mm)	Integration range	φ_g (mrad)	φ (mrad)	Reduction (%)
Circular, $r=0.18$	0.063	$2\sigma_B$	0.322	0.284	11.9
		$3\sigma_B$		0.279	13.3
		$5\sigma_B$		0.278	13.6
		$3\sigma_B$	0.500	0.474	5.2
Rectangular, 0.37×1.00		$3\sigma_B$	1.000	0.995	0.5

The time correlation between the detection of a scattered proton and an ion depends on the charge-to-mass ratio q/m for the ion. In Fig. 3(a) we show a typical spectrum of pulses from the TAC for ionization of Ne gas. A constant extraction field was used in the gas cell. The spectrum shows three peaks of real coincidences corresponding to the charge states 1 to 3 of ^{20}Ne and a satellite peak from $^{22}Ne^+$.

Differential cross sections for single ionization $d\sigma^+/d\Omega$ were obtained by the formula

$$\frac{d\sigma^+}{d\Omega}=\frac{N_C^+}{N_{\rm tot}}\frac{\sigma_{\rm tot}}{\Omega}\ , \tag{2}$$

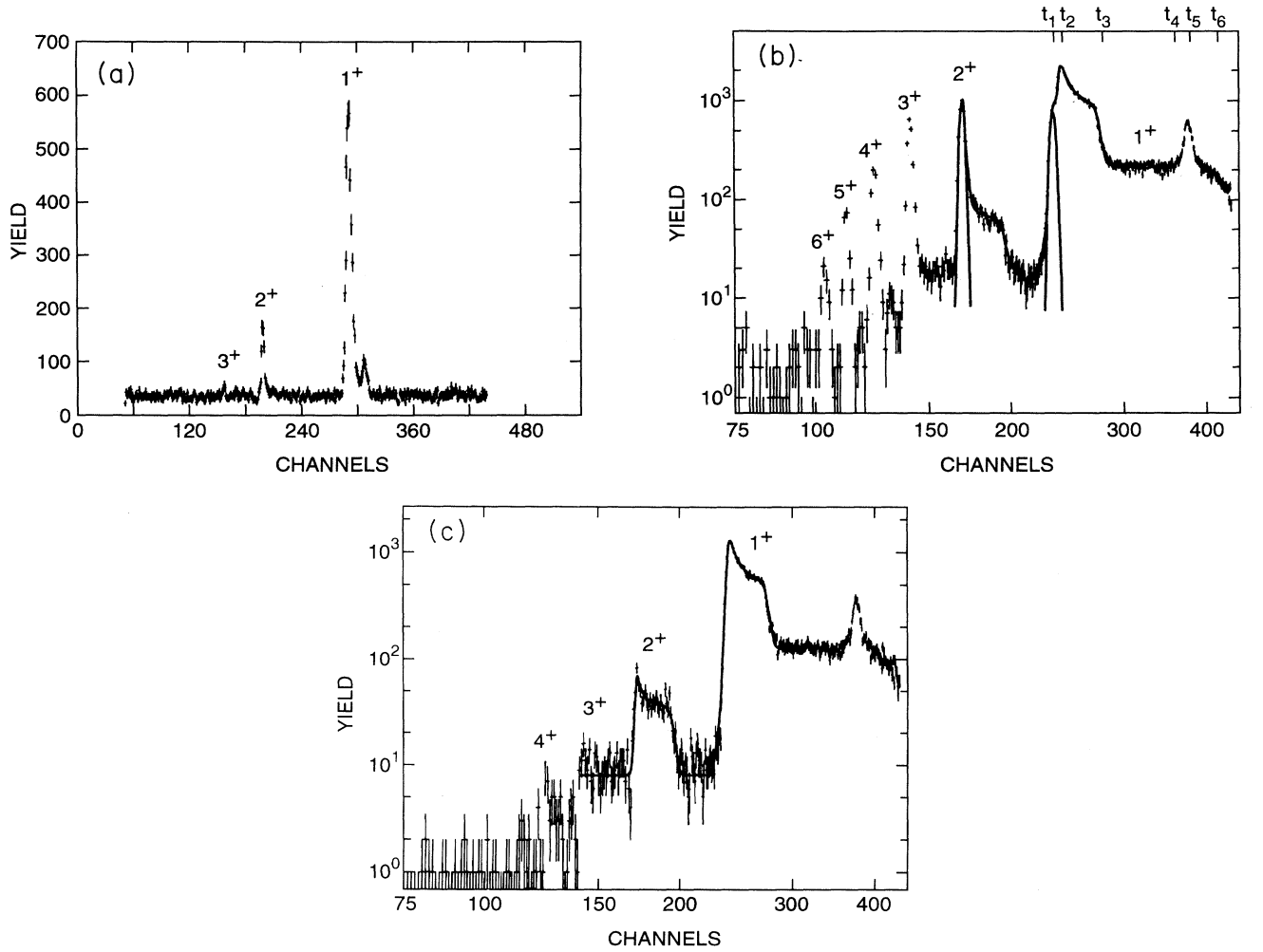

FIG. 3. (a) Spectrum of coincidences between scattered protons and Ne^{q+} for 1-MeV protons on Ne. Proton deflection angle, 1.00 mrad. Constant ion-extraction field. Peaks from charge states 1 to 3 of ^{20}Ne as well as from $^{22}Ne^+$ are seen above the random background. (b) Spectrum of coincidences between scattered protons and $^{40}Ar^{q+}$ for 1-MeV protons on Ar. Proton deflection angle, 2.36 mrad. Pulsed ion-extraction field. The spectrum shows coincidence structures for the ions $^{40}Ar^{q+}$, with $q=1-6$. The curves are random backgrounds taken from (c), and Gaussian peaks of real coincidences. The detailed structure of the spectrum is discussed in the text. A double-logarithmic plot is used to bring out the small charge states. (c) Same as (b), except that the TAC was started by a test pulser running at 400 Hz. The curves show random coincidences used in analyzing the spectra in (b).

where N_C^+ is the number of real coincidences with singly charged ions obtained in a given measurement, N_{tot} is the corresponding total number of extracted ions, σ_{tot} is the total ionization cross section which is taken from the literature [11], and Ω is the solid angle of the proton detector given by the area A of the aperture in front of the detector and the distance R to the gas cell ($\Omega = A/R^2$). The areas of the apertures were measured relative to a larger area which could be determined accurately by use of a microscope by carefully measuring the relative amounts of light from a homogeneous beam transmitted through the different apertures.

Spectra such as the one shown in Fig. 3(a) also yield ratios

$$R_q = \frac{N_C^{q+}}{N_C^+} = \frac{d\sigma^{q+}/d\Omega}{d\sigma^+/d\Omega} = \frac{d\sigma^{q+}}{d\sigma^+} \tag{3}$$

between differential multiple- and single-ionization cross sections for small values of q (i.e., $q=2$ and 3). The quantity N_C^{q+} is the number of real coincidences with ions of charge state q. Higher-charge states are masked by random coincidences primarily from singly charged ions.

This masking of the high-charge states can be avoided by using a pulsed extraction field instead of a constant field in the gas cell. This is seen in Fig. 3(b), which for an Ar target shows charge states 1 through 6 with very little random background near the high-charge states. The spectrum was obtained as follows: A small field (-2 V, 0 V; 4 V/cm) was maintained in the gas cell antiparallel to the direction of the extraction system to continuously clean the gas cell for ions. This reverse field, however, was suddenly (25 nsec rise time) replaced for 4 μsec by a field in the direction of the extraction system (-2 V, -22 V; 40 V/cm) whenever a scattered proton was detected by the SB detector. The rather complicated shape of the spectrum of singly charged ions may be understood as follows: The broad structure to the left is composed of a narrow peak of real coincidences at time t_1 and a background of random coincidences from times t_2 to t_3 due to singly charged ions already present in the gas cell when the extraction field is turned on. These ions are found between the beam axis (time t_2) and the far side of the gas cell relative to the extraction system (time t_3). The peak of real coincidences at t_1 is shifted relative to the peak in the random spectrum at t_2 due to the collision-induced recoil velocity of the coincident ions. The flat part of the spectrum between times t_3 and t_4 shows normal random coincidences. This background would be present throughout the spectrum in an experiment with a constant extraction field. When the extraction field is turned off at time t_6, the ions close to the near side of the gas cell are suddenly raised to a higher potential. Among these ions, those that have already left the gas cell experience an extra acceleration in the direction of the extraction and form a peak at time t_5. The remainder is slowed down by the reverse field, but some have enough kinetic energy to escape and form a long tail in the spectrum at times $t > t_6$. This complicated background is repeated in all the charge states but the size of it relative to the real coincidences quickly decreases as the charge state is increased. In order to be able to subtract reliably the backgrounds, pure background spectra were measured by substituting the pulses from the proton detector (SB in Fig. 1) by the pulses from a test-pulser running at 400 Hz. A spectrum obtained with this technique is shown in Fig. 3(c). The shape of the spectrum was modeled analytically and used to subtract the background as illustrated in Fig. 3(b). The real coincidences N_C^{q+} obtained in this way were used to determine the ratios

$$F_{2+}^{q+} = \frac{N_C^+}{N_C^{2+}} = \frac{d\sigma^{q+}}{d\sigma^{2+}} \tag{4}$$

for $q=3$–6. When combined with values of $R_2 = d\sigma^{2+}/d\sigma^+$ from constant-field measurements, a set of ratios $R_q = d\sigma^{q+}/d\sigma^+$ for $q=2$–6 was obtained.

Ratios between total cross sections for single σ^+ and multiple σ^{q+} ionization $q=2$–3 were derived from the background spectra [Fig. 3(c)] by the relation

$$R_q^{\text{tot}} = \frac{N_C^{q+}}{N_C^+}\sqrt{q} = \frac{\sigma^{q+}}{\sigma^+} , \tag{5}$$

where N_C^{q+} and N_C^+ are the number of counts for charge states q and 1, respectively, and the factor $\sqrt{q}$ corrects

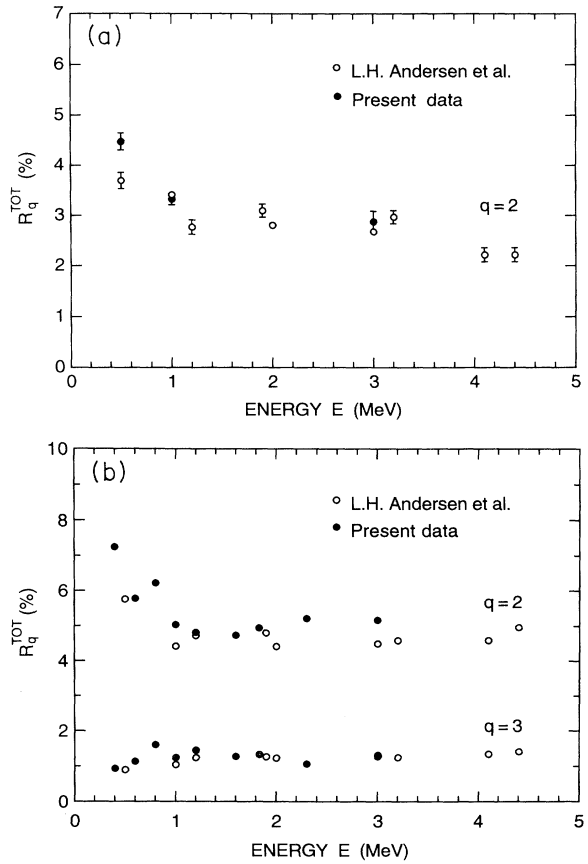

FIG. 4. Ratios $R_q^{\text{tot}} = \sigma^{q+}/\sigma^+$ between total cross sections for multiple and single ionization of (a) Ne and (b) Ar by protons. ●, present data; ○, Andersen *et al.* [3].

for the charge-state-dependent time that an ion spends in the gas cell while it drifts towards the far side of the cell under the influence of the small electric field used to remove most noncoincident ions. Experimental values of the ratios R_q^{tot} have been published earlier [3]. In this experiment, they are extracted only for comparison with the earlier data. The result is shown in Fig. 4. The excellent agreement supports our understanding of the details of the pulsed extraction.

RESULTS AND DISCUSSION

The measured differential single-ionization cross section $d\sigma^+/d\Omega$ for protons on Ne and Ar are shown in Figs. 5 and 6, respectively, as functions of the deflection angle φ of the proton. The cross sections lie approximately on straight lines in these double-logarithmic plots. This shows that the angular variation for constant projectile energy E is given approximately by a power law

$$\frac{d\sigma^+}{d\Omega} \propto \frac{1}{\varphi^k} , \tag{6}$$

where k is near 3.8 for Ne and 3.65 for Ar with only a weak dependence of k on the projectile energy.

The energy dependence of $d\sigma^+/d\Omega$ for constant $E\varphi = 2.6$ MeV mrad is shown in Fig. 7. A constant $E\varphi$ translates into an approximately constant impact parameter p which for the present value of $E\varphi$ is $0.91a_K$ for Ne and $1.04a_L$ for Ar where a_K and a_L are the radii of the K and L shells, respectively. The connection between φ and p was found by assuming classical elastic scattering in a screened Coulomb potential [12]. For the K-shell radius of Ne, we used $a_K = a_0/(10-0.3)$, where a_0 is the Bohr radius and for the L-shell radius of Ar $a_L = 2a_0/(18-4.15)$. One sees from Fig. 7 that also the energy dependence for constant $E\varphi$ is given approximately by a power law

$$\frac{d\sigma^+}{d\Omega} \propto E^p , \tag{7}$$

where p is close to 1.3 for both gases. The total scattering cross section $d\sigma_{sc}/d\Omega$ at the above constant impact parameter increases approximately as E^2, which shows that the single-ionization probability defined as

$$P = \frac{d\sigma^+/d\Omega}{d\sigma_{sc}/d\Omega} \tag{8}$$

decreases with E like $1/E^{0.7}$ for both gases at the present energies and impact parameters.

Figure 8 shows small-angle values of $d\sigma^+/d\varphi$ for Ne and Ar at $E = 3$ MeV compared with the data by Kamber *et al.* [6]. The agreement is quite satisfactory, especially near 0.5 mrad where the precision is highest for both gases. However, the present data do seem to be systematically larger than the previous ones by about 30% in the region 0.60–0.95 mrad.

Measured ratios $R_q = d\sigma^{q+}/d\sigma^+$ between multiple- and single-ionization cross sections for protons on Ne as a function of deflection angle are shown at three energies in Fig. 9. For each energy, we have marked the angle corresponding to an impact parameter equal to the K-

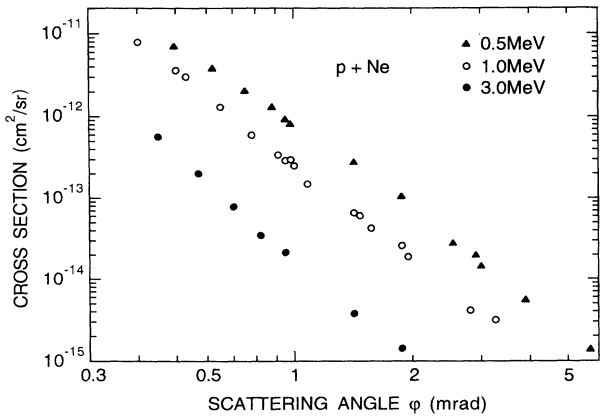

FIG. 5. Differential single-ionization cross section $d\sigma^+/d\Omega$ for 0.5-, 1.0-, and 3.0-MeV protons on Ne as a function of the scattering angle φ of the proton in the laboratory frame.

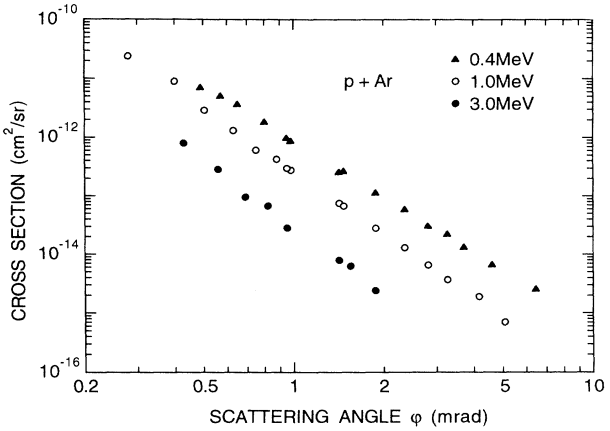

FIG. 6. Differential single-ionization cross section $d\sigma^+/d\Omega$ for 0.4-, 1.0-, and 3.0-MeV protons on Ar as a function of the scattering angle φ of the proton in the laboratory frame.

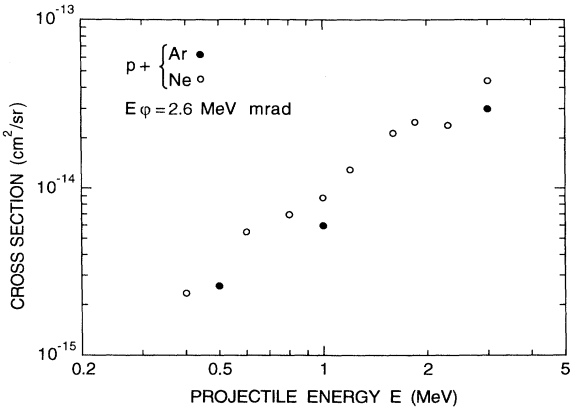

FIG. 7. Differential single-ionization cross sections $d\sigma^+/d\Omega$ for protons on Ne and Ar as a function of proton energy E for constant $E\varphi = 2.6$ MeV mrad.

shell radius. The ratios R_2 rise relatively fast in the interval 0.5–1.0 mrad corresponding to distant collisions and then saturate for closer collisions with impact parameters of the order of the K-shell radius. The ratios R_q with $q=3$ or 4 increase significantly in the entire angular region covered experimentally. The rise is as high as a factor of 20 for $q=4$ at 1 MeV.

The above behavior is reproduced qualitatively by an empirical model calculation in which it is assumed that (i) the ionization probability for each L-shell electron is constant, independent of the degree of ionization, (ii) the multiple ionization is described by a binomial distribution, (iii) the differential multiple-ionization cross sections for the L shell may be expressed as a probability factor times a common scattering cross section $d\sigma_{sc}/d\Omega$, and (iv) the ionization of a K-shell electron leads to further ionization due to radiationless transitions and shakeoff. The model calculation is similar to those by Kamber *et al.* [6] and Sharabati *et al.* [7].

Within this model, the differential cross section for direct ionization of q L-shell electrons is given by the expression

$$\frac{d\sigma_L^{q+}}{d\Omega}=\binom{8}{q}p_L^q(1-p_L)^{8-q}\frac{d\sigma_{sc}}{d\Omega}=P_L(q)\frac{d\sigma_{sc}}{d\Omega}\ , \tag{9}$$

where p_L is the ionization probability for each L-shell electron and $P_L(q)$ is the probability for q-fold ionization of the L shell at the given deflection angle. In terms of the *total* cross section for q-fold ionization $d\sigma^{q+}/d\Omega$ and the K-shell-ionization cross section [13] $d\sigma_{KI}/d\Omega$, the same cross section is given by

$$\frac{d\sigma_L^{q+}}{d\Omega}=\frac{d\sigma^{q+}}{d\Omega}-\sum_{i=1}^{q}P_L(q-i)f_i^{so}\frac{d\sigma_{KI}}{d\Omega}\ , \tag{10}$$

where f_i^{so} is the probability that a single K-shell ioniza-

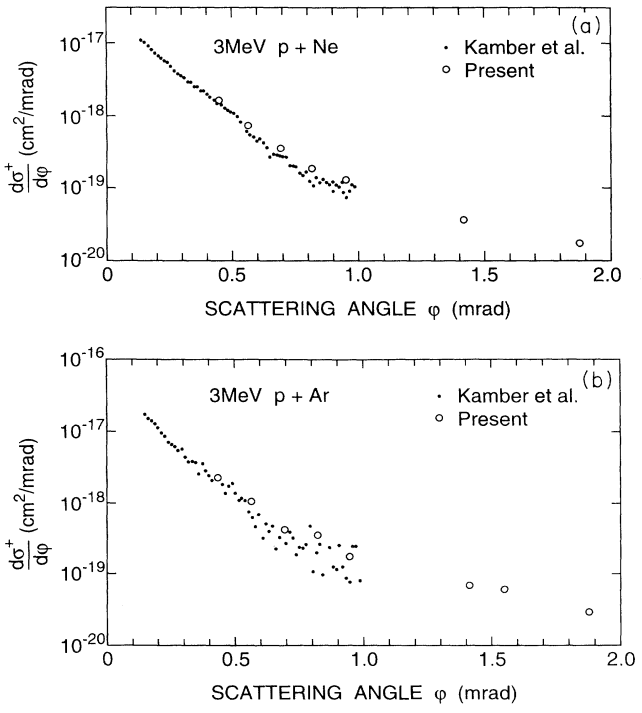

FIG. 8. The present differential single-ionization cross sections $d\sigma^+/d\varphi=2\pi\varphi d\sigma^+/d\Omega$ as functions of the scattering angle φ for protons on (a) Ne and (b) Ar compared with previous measurements by Kamber *et al.* [6].

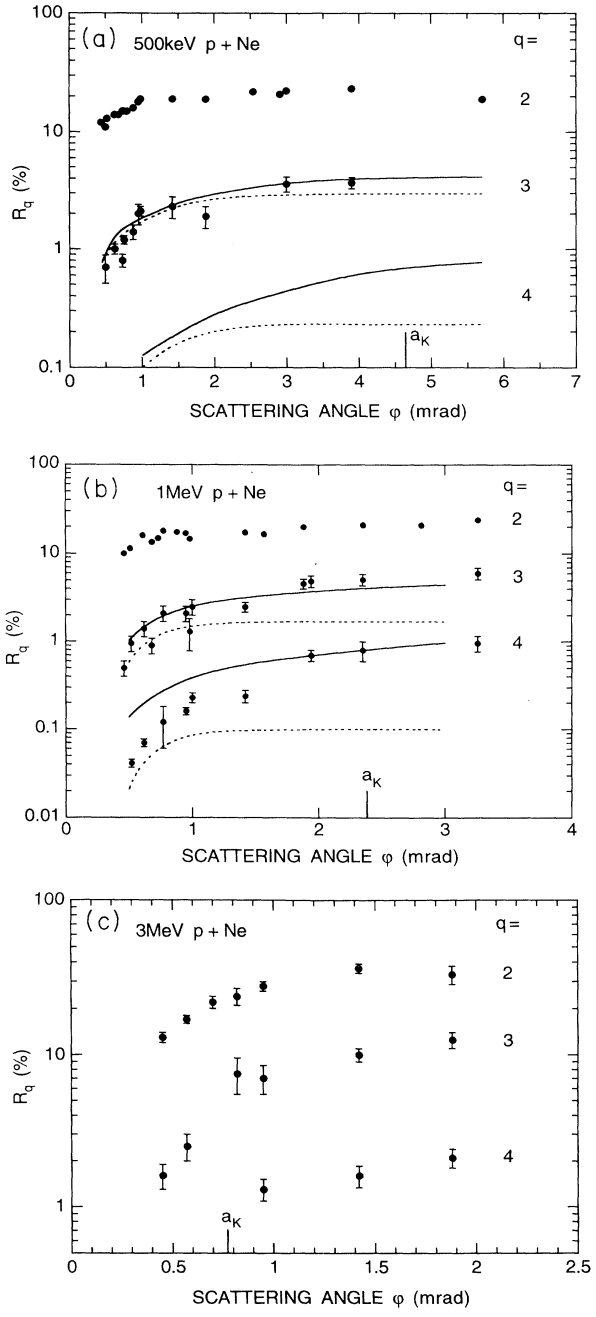

FIG. 9. Ratios $R_q=d\sigma^{q+}/d\sigma^+$ between differential cross sections for multiple and single ionization of Ne by protons. (a) $E_p=0.5$ MeV. (b) $E_p=1.0$ MeV. (c) $E_p=3.0$ MeV. Continuous curve, semiempirical model calculation for $q=3$ and 4; dotted curve, pure L-shell contribution.

tion leads to charge state i as a result of radiationless transitions [14] (shakeoff).

As a first step of an iterative determination of the probabilities p_L we set these quantities equal to zero on the right-hand side of Eq. (10). This leads to

$$\frac{d\sigma_L^+}{d\Omega}=\frac{d\sigma^+}{d\Omega}-f_1^{\rm so}\frac{d\sigma_{KI}}{d\Omega} \tag{11}$$

and

$$\frac{d\sigma_L^{2+}}{d\Omega}=\frac{d\sigma^{2+}}{d\Omega}-f_2^{\rm so}\frac{d\sigma_{KI}}{d\Omega} \tag{12}$$

where all quantities on the right-hand sides are known experimentally. Therefore the ratio

$$R_2^L=\frac{d\sigma_L^{2+}/d\Omega}{d\sigma_L^+/d\Omega} \tag{13}$$

can be determined and, using Eq. (9), we find

$$p_L=\frac{2R_2^L}{7+2R_2^L} \tag{14}$$

as a first approximation for p_L. When this value is used in Eq. (10) with $q=1$ and 2, improved values for R_2^L and p_L follow. Two iterations are sufficient to determine p_L. Once this is done, it is possible to find the scattering cross section [Eq. (9)],

$$\frac{d\sigma_{\rm sc}}{d\Omega}=\frac{1}{8p_L(1-p_L)^7}\frac{d\sigma_L^+}{d\Omega} \tag{15}$$

and, using Eqs. (9) and (10), the pure L-shell ionization cross section $d\sigma_L^{q+}/d\Omega$, and the total ionization cross section $d\sigma^{q+}/d\Omega$ for $q=3$ and 4. Ratios $R_q^L=d\sigma_L^{q+}/d\sigma_L^+$ and $R_q=d\sigma^{q+}/d\sigma^+$ between these cross sections and $d\sigma_L^+/d\Omega$ and $d\sigma^+/d\Omega$, respectively, are shown in Fig. 9. The model clearly describes the qualitative features quite well (see also Fig. 12), but some deviation at small deflection angles is also seen. At 1 MeV, K-shell ionization contributes strongly to the multiple ionization in the full range of deflection angles. At 500 keV, K-shell ionization is important only for close collisions.

The experimental single-electron ionization probabilities p_L for the L shell found by use of the model are shown in Fig. 10. The probabilities increase strongly at small deflection angles, but approach constant values within experimental error at the largest angles, corresponding to impact parameters of the order of the K-shell radius and thus small compared to the L-shell radius. The probabilities are compared to earlier data by Sharabati *et al.* [7] derived by simultaneously fitting *all* charge-state components with the two parameters p_L and p_K. This leads to values of p_L and p_K which are smaller than those found by us. The different procedures used may account for this discrepancy.

Figure 11 shows measured ratios $R_q=d\sigma^{q+}/d\sigma^+$ between multiple- and single-ionization cross sections for protons on Ar as functions of deflection angle at three energies. The multiple ionization is clearly much stronger for Ar than for Ne. Nevertheless, the qualitative

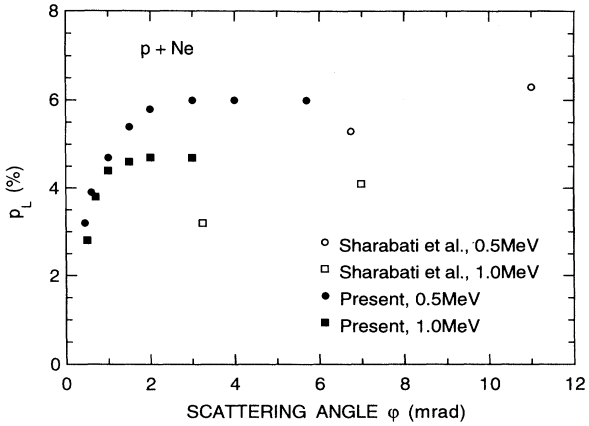

FIG. 10. Single-particle ionization probabilities p_L for L-shell electrons of Ne by protons as a function of the scattering angle of the proton in the laboratory frame. Present data: ●, $E_p=0.5$ MeV; ■, $E_p=1.0$ MeV. Sharabati *et al.* [7]: ○, $E_p=0.5$ MeV; □, $E_p=1.0$ MeV.

behavior of the cross-section ratios is very similar. The lack of experimental differential L-shell ionization cross sections prevents a more detailed analysis of the data along the lines used for Ne, but there is only little doubt that single and double ionization in the most distant collisions are dominated by pure M-shell ionization and that L-shell ionization followed by Auger and Coster-Kronig transitions is responsible for most of the multiple ionization in close collisions.

The assumptions behind the model used for the description of the multiple ionization of Ne undoubtedly represent an oversimplification, as seen from the lack of detailed agreement with the data. In particular, assumption (i) does not seem to be very realistic when a large fraction of electrons is removed from a given shell, and assumption (ii) depends on (i), and it further requires uncorrelated electrons. Theoretical approaches avoiding some of these restrictions are being developed [2,15].

In Figs. 12 and 13, the present ratios between multiple-ionization cross sections are compared with previous data by Sharabati *et al.* [7] for Ne at 0.5 and 1.0 MeV, and by Kamber *et al.* [6] for Ne and Ar at 3 MeV, respectively. Sharabati *et al.* [7] presented their data in the form of impact-parameter-dependent ionization probabilities. The impact parameters were calculated from measured deflection angles by use of an exponentially screened Coulomb potential [16]. The authors state that for the most distant collisions, the derived impact parameters deviate by up to 10% from those found using an unscreened Coulomb potential. Since the ratios between the probabilities depend only weakly on impact parameter, we translated impact parameters back to deflection angles by use of pure Rutherford scattering off the Ne nucleus. This means that the smallest deflection angles were in reality up to 10% smaller than indicated in Fig. 12. Even with this uncertainty, it is clear that the two sets of data join each other smoothly. For Ne and Ar at 3 MeV, however, as seen in Fig. 13, there is clearly a serious disagreement in absolute magnitude, but the angular vari-

ations do not seem to differ much. In view of the otherwise good agreement between the present and previous data (Figs. 4 and 12), we tend to believe that the data of Kamber *et al.* [6] suffer from an error. The experimental techniques and methods of data reduction used by Kamber *et al.* [6] are very similar to ours, but some difference exists in the details. It is not clear from the description of the experimental method [6] what the potential difference ΔV between the target and the microchannel plate used to detect recoil ions was. If a small value [$\Delta V < (2-3)$ kV] was used, the detection efficiency may have increased strongly with increasing charge state and decreasing mass [3]. If this were the case, it would result in a relative overestimation of multiple-ionization cross sections for both gases but more for Ar than for Ne. This is precisely what is seen (Fig. 13). We mentioned earlier that the agreement between experimental values for the differential single ionization cross section $d\sigma^+/d\Omega$ obtained by Kamber *et al.* [6] and that in the present experiment is satisfactory. This does not contradict the above conclusion because in both experiments, the number of real coincidences between scattered protons and singly charged recoil ions is normalized to the total number of recoil ions [Eq. (2)], which is dominated by singly charged ions (see Fig. 4). The value of the derived differential single-ionization cross section therefore does not depend on the detection efficiency for recoil ions, but only on a common total-ionization cross section [11] and the solid angle and efficiency (very close to 1) of the solid-state surface-barrier detectors used in both experiments to count scattered protons.

Experimental differential scattering cross sections obtained from Eq. (15) are shown in Fig. 14. The data are

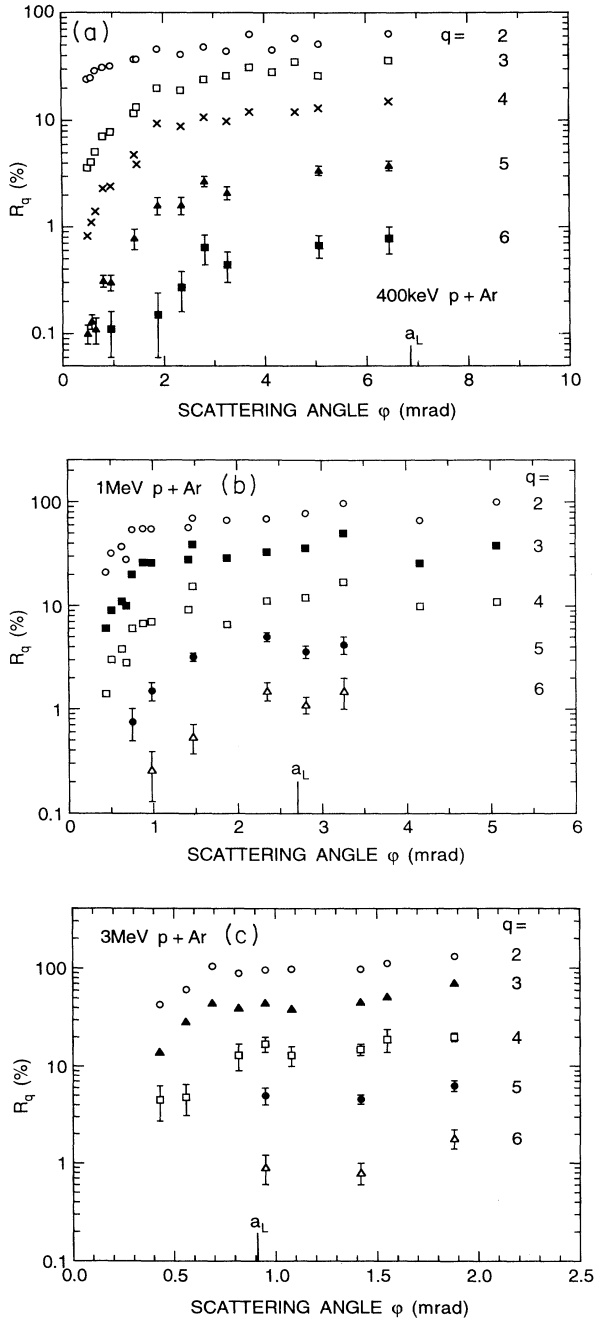

FIG. 11. Ratios $R_q = d\sigma^{q+}/d\sigma^+$ between differential cross sections for multiple and single ionization of Ar by protons. (a) $E_p = 0.4$ MeV. (b) $E_p = 1.0$ MeV. (c) $E_p = 3.0$ MeV.

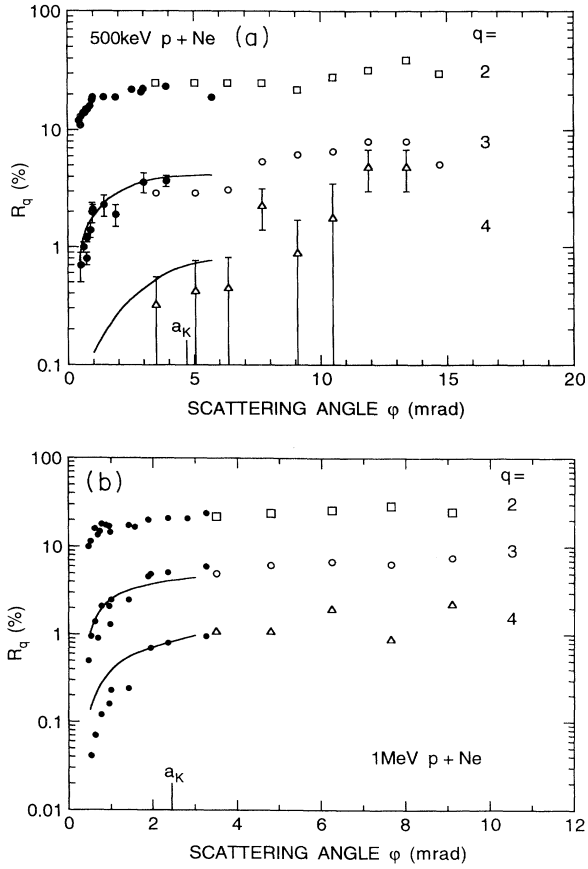

FIG. 12. Ratios $R_q = d\sigma^{q+}/d\sigma^+$ between differential cross sections for multiple and single ionization of Ne by protons. ●, present data; □, ○, △, Sharabati *et al.* [7]. (a) $E_p = 0.5$ MeV. (b) $E_p = 1.0$ MeV.

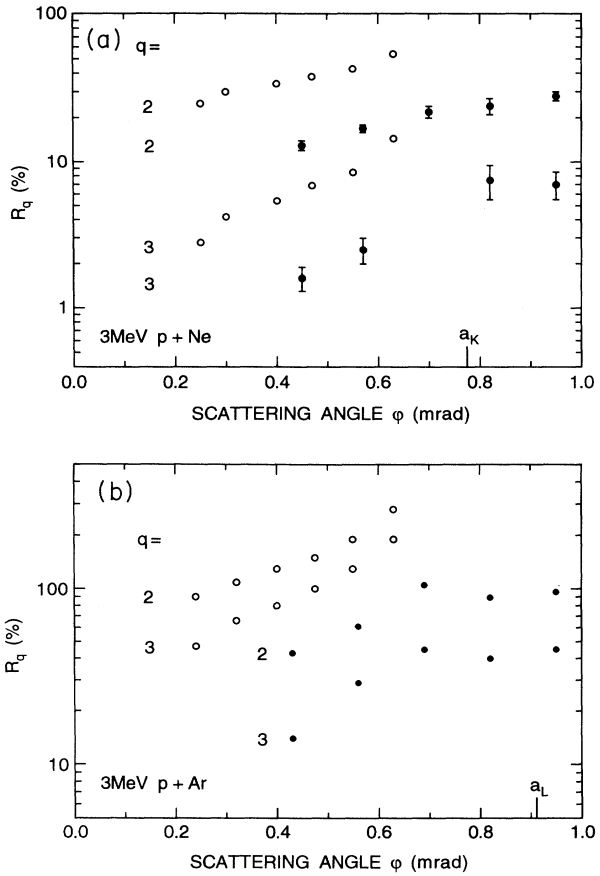

FIG. 13. Ratios $R_q = d\sigma^{q+}/d\sigma^{+}$ between differential cross sections for multiple and single ionization by 3.0-MeV protons. ●, present data; ○, Kamber *et al.* [6]. (a) Ne target. (b) Ar target.

presented in the form of reduced cross sections as functions of reduced deflection [12] to facilitate comparison between the two sets of experimental data and theoretical estimates. With the scaling parameters used, the data should approximately follow a universal curve [12] which is estimated by three screened model potentials. The reduced cross sections lie indeed on a common curve for $t^{1/2}$ values of the order of unity, but they deviate from each other and are much higher than model calculations at lower values of $t^{1/2}$. Such a behavior is not seen for heavy-ion impact [17]. The lowest $t^{1/2}$ values for the two sets of experimental data correspond to a deflection angle of about 0.5 mrad (Fig. 9), which is smaller than the maximum deflection angle of 0.55 mrad for a proton off a free electron at rest. The large values of the reduced cross sections and the lack of scaling for deflection angles near 0.5 mrad may thus be due to binary collisions between the projectile and target electrons [18].

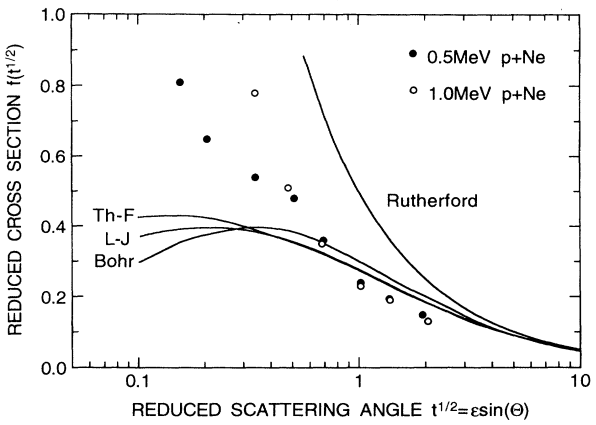

FIG. 14. Total differential scattering cross sections $d\sigma_{sc}/d\Omega$ for protons on Ne in reduced units [12]. ●, $E_p = 0.5$ MeV; ○, $E_p = 1.0$ MeV. Theoretical curves for elastic scattering: Rutherford (RF); screened potentials: Thomas-Fermi (Th-F), Lenz-Jensen (L-J), and exponential (Bohr).

CONCLUSIONS

Experimental cross sections for single and multiple ionization of Ne and Ar by fast protons have been obtained. The cross sections are differential in the proton deflection angle and cover an angular region wide enough to display the transition from distant to close collisions.

The experimental results form a bridge between two previous sets of data. One set covers relatively low energies and close collisions, while the other covers high energies and distant collisions. The three sets of experimental data supplement one another, and they are consistent with each other except for one result discussed in the text.

A semiempirical model calculation has helped in the interpretation of the data on multiple ionization, but a detailed understanding requires an improved analysis.

ACKNOWLEDGMENTS

The support of A.D.G. by the Danish Natural Science Research Council (SNF) is gratefully acknowledged.

[1] F. Hopkins, D. O. Elliott, C. P. Bhalla, and P. Richard, Phys. Rev. A **8**, 2952 (1973).

[2] R. L. Becker, A. L. Ford, and J. F. Reading, Nucl. Instrum. Methods B **10/11**, 1 (1985).

[3] L. H. Andersen, P. Hvelplund, H. Knudsen, S. P. Møller, A. H. Sørensen, K. Elsener, K.-G. Rensfelt, and E. Uggerhøj, Phys. Rev. A **36**, 3612 (1987).

[4] J. C. Levin, D. W. Lindle, N. Keller, R. D. Miller, Y. Azuma, N. Berrah Mansour, H. G. Berry, and I. A. Sellin, Phys. Rev. Lett. **67**, 968 (1991); A. Dalgarno and H. R. Sadeghpour, Phys. Rev. A **46**, R3591 (1992); R. J. Bartlett, P. J. Walsh, Z. X. He, Y. Chung, E-M Lee, and J. A. R. Samson, *ibid.* **46**, 5574 (1992); J. C. Levin, I. A. Sellin, B. M. Johnson, D. W. Lindle, R. D. Miller, N. Berrah, Y. Azuma, H. G. Berry, and D.-H. Lee, *ibid.* **47**, R16 (1993).

[5] M. O. Krause and T. A. Carlson, Phys. Rev. **158**, 18 (1967).

[6] E. Y. Kamber, C. L. Cocke, S. Cheng, and S. L. Varghese,

Phys. Rev. A **41**, 150 (1990).
[7] H. Sharabati, K. Bethge, J. Ullrich, R. Dörner, R. E. Olson, V. Dangendorf, R. Koch, and H. Schmidt-Böcking, J. Phys. B **23**, 2957 (1990).
[8] G. Schiwietz, Phys. Rev. A **37**, 370 (1988); B. Skogvall and G. Schiwietz, *ibid.* **46**, 5687 (1992).
[9] E. Y. Kamber, C. L. Cocke, S. Cheng, and S. L. Varghese, Phys. Rev. Lett. **60**, 2026 (1988); E. Y. Kamber, C. L. Cocke, S. Cheng, J. H. McGuire, and S. L. Varghese, J. Phys. B **21**, L455 (1988).
[10] F. G. Kristensen and E. Horsdal-Pedersen, J. Phys. B **23** 4129 (1990).
[11] M. E. Rudd, Y. K. Kim, D. H. Madison, and J. W. Gallagher, Rev. Mod. Phys. **57**, 965 (1985).
[12] J. Lindhard, V. Nielsen, and M. Scharff, K. Dan. Vidensk. Selsk. Mat. Fys. Medd. **36**, No. 10, 1 (1968).
[13] E. Horsdal-Pedersen, F. Folkmann, and N. H. Pedersen, J. Phys. B **15**, 739 (1982).
[14] T. A. Carlson, W. E. Hunt, and M. O. Krause, Phys. Rev. **151**, 41 (1966).
[15] M. Horbatsch, J. Phys. B **22**, L639 (1989); Comput. Phys. Commun. **63**, 115 (1991).
[16] R. Dörner (private communication).
[17] P. Loftager, F. Besenbacher, A. S. Jensen, and V. S. Sørensen, Phys. Rev. **20**, 1443 (1979).
[18] P. Loftager (private communication).